Food Chemistry: X 27 (2025) 102395

Contents lists available at ScienceDirect

Food Chemistry: X

journal homepage: www.sciencedirect.com/journal/food-chemistry-x

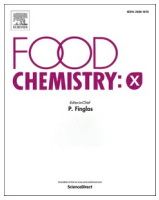

# Trash to treasure: Potential antifreeze peptide from *Litopenaeus vannamei* head *via* ultrasound-assisted autolysis

Mingtang Tan [a,b,c,d,1], Mei Han [a], Yingyu Zhou [a], Zhongqin Chen [a,b,c,d], Wenhong Cao [a,b,c,d,*]

[a] College of Food Science and Technology, Guangdong Ocean University, Zhanjiang 524088, China
[b] National Research and Development Branch Center for Shellfish Processing (Zhanjiang), Zhanjiang 524088, China
[c] Guangdong Provincial Key Laboratory of Aquatic Products Processing and Safety, Guangdong Provincial Engineering Technology Research Center of Seafood, Zhanjiang 524088, China
[d] Shenzhen Institute of Guangdong Ocean University, Shenzhen 518108, China

ARTICLE INFO

*Keywords:*
Shrimp head autolysate
Antifreeze peptides
Bioinformatic
Molecular dynamics simulation
Antifreeze mechanism

ABSTRACT

This study aimed to separate and purify antifreeze peptides (AFP) from the autolysate of *Litopenaeus vannamei* head, and the peptide sequences with antifreeze activity were identified to elucidate the potential antifreeze mechanisms. The initial fractionation of autolysate revealed that the pk1 fraction with less than 3 kDa molecular weight exhibited the highest thermal hysteresis activity (2.28 °C). Notably, the component pk1-A with the strongest antifreeze activity (2.80 °C) was further separated by using a Sephadex G-15 gel filtration column. The results of bioinformatics and computer-assisted techniques indicated that 26 types of peptides from pk1-A were identified as AFP. Among these, KQVHPDTGISSK was selected as a potential *Litopenaeus vannamei* head antifreeze peptide (LvAFP). The active site (Lys residue) of LvAFP was discovered to strongly interact with water molecules *via* hydrogen bonding, thereby inhibiting the formation and recrystallization of ice crystals. Therefore, the preparation of LvAFP could improve the high-value utilization of shrimp byproducts.

## 1. Introduction

It is well known that aquatic products are highly susceptible to microbial contamination after harvesting, which leads to spoilage and reduced nutritional value, thereby shortening shelf life. Freezing is one of the oldest and most widely employed food preservation methods, which can extend the shelf life and maintain the quality of aquatic products (Sun, Zhang, Yang, et al., 2023). Nevertheless, ice crystal formation may irreversibly cause quality deterioration of aquatic products during freezing, such as changes in texture, color, and flavor. Additionally, protein denaturation and oxidation are aggravated by freeze-thaw cycles during transportation or distribution (Chu, Ding, Wang, Xie, & Ding, 2023). Therefore, it is essential to inhibit the formation and recrystallization of ice crystals to maintain the frozen quality of food (Tan, Ye, Chu, & Xie, 2021).

Cryo-protectants play a significant role in enhancing the water-holding capacity of aquatic products and effectively attenuating the protein freezing denaturation during freezing (Cao et al., 2023; Yu et al., 2022). Traditional and commercial cryo-protectants include sugars, polyphosphate, and their complexes (Cao et al., 2023). Although these cryo-protectants present excellent antifreeze efficiency and low-cost, they can negatively affect the flavor of aquatic products and raise health concerns. In contrast, antifreeze peptides (AFP) are low-molecular weight protein hydrolysates with a strong thermal hysteresis (TH) capability, which inhibit the ice crystal growth, hinder recrystallization induced by freeze-thaw cycles, and regulate ice crystal morphology (Yang et al., 2023). Recent studies have revealed that various protein hydrolysates prepared from aquatic products or their byproducts, such as silver carp (*Hypophthalmichthys molitrix*) (Cui et al., 2023), tilapia (Cao et al., 2023), crayfish shells (Liu et al., 2024), takifugu obscurus (Yang et al., 2022), sturgeon (Wang et al., 2024) and large yellow croaker (Xu et al., 2024) exhibit cryo-protective capabilities. The antifreeze activity of collagen hydrolysates has been intensively investigated, suggesting that the peptides containing unique repeating Gly-XY sequences and molecular weights of 1000–3000 Da typically exhibit antifreeze potential (Dang et al., 2022).

* Corresponding author at: College of Food Science and Technology, Guangdong Ocean University, Zhanjiang 524088, China
*E-mail addresses:* mttan@gdou.edu.cn (M. Tan), cwenhong@gdou.edu.cn (W. Cao).
[1] First author.

https://doi.org/10.1016/j.fochx.2025.102395
Received 21 January 2025; Received in revised form 24 February 2025; Accepted 17 March 2025
Available online 21 March 2025

Pacific white shrimp (*Litopenaeus vannamei*) is popular among consumers due to its flavor and nutritional value. China harvested approximately 1.34 million tons of L. *vannamei* from marine aquaculture in 2022 (N'Souvi, Sun, Che, & Vodounon, 2024). Nevertheless, shrimp heads are frequently discarded as byproducts during consumption or processing, causing the loss of valuable bioactive components. Shrimp heads account for 35–45 % of the total weight and are rich in protein (50–65 %, dry weight basis) (Cao, Tan, Zhan, Li, & Zhang, 2014). Hence, the recovery of bioactive molecules from shrimp heads is beneficial in enhancing the profitability of shrimp processing and reducing environmental pollution. Moreover, enzymatic hydrolysis is commonly used to extract protein from aquatic byproducts (Tadesse et al., 2023), but shrimp heads can undergo autolysis without external proteases due to their endogenous hydrolytic enzymes. Numerous studies have focused on extracting various compounds from shrimp heads, such as carotenoids (Dayakar et al., 2022), astaxanthin (El et al., 2024), and bioactive peptides (Nirmal, Santivarangkna, Rajput, & Benjakul, 2020). Relevant data also indicated that these active substances extracted could be served as non-toxic food additives (Nirmal et al., 2020). Zhu, Zheng, and Dai (2022) reported that byproducts autolysate of white-hair rough shrimp (*Trachypenaeus curvirostris*) exhibited significant antifreeze protection in shrimp muscles during freeze-thaw cycles. This effect was attributed to specific structures of low-molecular weight peptides that can bind to ice crystals through hydrogen bonding. More importantly, we recently identified a thermal hysteresis activity (THA) of 1.82 °C and a hydrolysis degree of 32.59 % in shrimp heads at specific autolysis conditions (50 °C, pH 7.0, 5 h) (Majura et al., 2023). As can be concluded, the autolysis hydrolysate of shrimp head shows a satisfactory antifreeze effect in aquatic products, but its development is limited by the long autolysis time and low hydrolysis degree. Ultrasound-assisted extraction is an effective extraction method for targeting active compounds, offering advantages such as higher extraction rate and shorter extraction time (Pacheco et al., 2024). In our preliminary pre-experiment, we found that ultrasound could promote shrimp head autolysis. The optimal ultrasound-assisted autolysis process conditions (ultrasound power of 300 W, ultrasound time of 15 min, pH 8.0, temperature of 50 °C, and autolysis time of 3 h) for shrimp heads was determined based on Plackett–Burman design experiment. Under these conditions, the hydrolysis degree of the shrimp head was 35.24 %. As is well known, the antifreeze mechanism of AFP is inseparably related to their amino acid composition, peptide sequence, and the ratio of hydrophilic to hydrophobic residues (Cui et al., 2023). The specific antifreeze mechanisms of AFP derived from shrimp heads prepared by ultrasound-assisted autolysis remain to be emphasized.

In this study, an ultrasound-assisted method was used to obtain shrimp head autolysates and explore structure-antifreeze activity relationship. Firstly, the autolysates were separated and purified using ultrafiltration and ion exchange chromatography. Subsequently, the fractions with high antifreeze activity were investigated for their cryoprotective effect on snakehead muscle during freeze-thaw cycles. We further obtained fractions with the highest antifreeze activity through gel chromatography and identified the peptide sequences with the utmost antifreeze potential using bioinformatics tools. Finally, the molecular docking technique was applied to investigate the binding mode and potential active sites between the antifreeze peptides and water molecules. The results of this study contribute to the development of effective AFP from shrimp head autolysate, providing valuable insights for high-value utilization of shrimp byproducts.

## 2. Materials and methods

### 2.1. Materials and reagents

Fresh Pacific white shrimp and snakehead were purchased from the Huguang market (Zhanjiang, China), and shrimp heads were collected. The Sephadex G-15 packing used in this study was obtained from Yuanye Co., Ltd. (Shanghai, China). While bovine serum albumin (BSA) was purchased from Solebo Technology Co., Ltd. (Beijing, China).

### 2.2. Preparation of shrimp head autolysate

The shrimp heads were homogenized at a material-liquid ratio of 1:5 (*w*:*v*) and autolyzed in a water bath at an ultrasound power of 300 W, ultrasound time of 15 min, pH of 8.0, temperature of 50 °C, and autolysis time of 3 h. After the reaction, the samples were transferred to a 100 °C water bath for 10 min to inactivate the enzyme, followed by cooling in an ice water bath. Finally, the sample was centrifuged under 4 °C at 9000 r/min for 15 min, and the supernatant was collected as the desired shrimp head autolysate.

### 2.3. Ultrafiltration fractionation and thermal hysteresis activity of autolysate

The prepared autolysate was diluted five times and filtered through a 0.45 μm filter membrane. Four molecular size fractions (<3 k, 3–5 k, 5–8 k, >8 kDa) were then separated by ultrafiltration membranes. The thermal hysteresis activity (THA)of each fraction was determined. The ultrafiltration fractions with the highest THA activity were collected, concentrated, lyophilized, and stored at −80 °C for later use.

The THA of each fraction was determined according to the method of Liang et al. (2025) with slight modifications. A 10 uL sample placed in an aluminum crucible was first cooled from room temperature to −25 °C at a rate of −5.0 °C/min, then heated to 25 °C at a rate of 5.0 °C/min. The melting enthalpy ($\Delta H_m$) was calculated from the heating curve. The sample was then immediately cooled from 25 °C to −25 °C at a rate of 5.0 °C/min and maintained for 1 min, followed by heating at 3.0 °C/min until an equilibrium state between ice crystals and aqueous solution was reached (holding temperature, $T_h$). Finally, the initial crystallization temperature ($T_0$) of the sample was recorded by decreasing to −25 °C at a rate of 3.0 °C/min, and the exothermic enthalpy of refreezing ($\Delta H_r$) was calculated. The THA of the sample was calculated as THA = $T_h$-$T_0$. Furthermore, the ice crystal content Φ (%) was estimated following an eq. (1).

$$\Phi(\%) = \left(1 - \frac{-\Delta H_r}{\Delta H_m}\right) \times 100 \quad (1)$$

### 2.4. Separation of high THA active fractions

After 10 mg/mL of high THA active fraction (<3 k) was ultra-filtered through a 0.22 μm filter membrane, separation was achieved using Capto Q anion-exchange chromatography (X. Zhang et al., 2024). The sample was eluted in a gradient phase with 0.01 M Tris-HCl containing 1.0 M NaCl at pH 8.0 at a flow rate of 5.0 mL/min. The eluate of each fraction was automatically collected based on peak detection when the absorbance at 220 nm reached a baseline tangent slope of 50. The THA and amino acid composition of each eluate fraction were determined. The obtained high THA eluate (pk1) was utilized in subsequent freeze-thaw cycling experiments for snakehead.

### 2.5. Determination of thermal hysteresis activity and amino acid composition for separation products

The thermal hysteresis activity (THA) of the separation product was consistent with section 2.3. The amino acid analysis of separation products was conducted according to the method described by Majura et al. (2023). The lyophilized samples were hydrolyzed with 6.0 mol/L HCl at 110 °C for 24 h. The samples were filtered through a 0.45 μm filter and analyzed by an Agilent 1100 HPLC system (Agilent, Palo Alto, CA).

### 2.6. Cryo-protective effect of pk1 fraction on snakehead muscle during freeze-thaw cycles

#### 2.6.1. Freeze-thaw cycle of snakehead muscle samples

The muscle from snakehead back fillets was obtained to make surimi and divided into five groups (Cao et al., 2023; Majura et al., 2024): (1) NC (negative control, surimi immersed in distilled water); (2) PC (positive control, surimi immersed in 0.5 % complex phosphate); (3) 0.5 % pk1 (surimi immersed in 0.5 % pk1 (*w/v*)); (4) 1.0 % pk1 (surimi immersed in 1.0 % pk1); (5) 3.0 % pk1 (surimi immersed in 3.0 % pk1). The five groups of samples were immersed for 2.0 h at 4 °C. Subsequently, the samples were stored at −20 °C for 72 h and then thawed at 25 °C. The freeze-thaw (F-T) cycle process was repeated five times. Additionally, snakehead fillets were immersed in the above solution for 4.0 h, and the microstructures of fillets were observed after each F-T cycle.

#### 2.6.2. Determination of total sulfhydryl content and surface hydrophobicity

Myofibrillar protein (MP) was extracted using the method described by Zhou et al. (2024). The MP content was measured using the Biuret method (Tan, Ye, & Xie, 2021). The total sulfhydryl content of MP was evaluated based on a total sulfhydryl group assay kit (Beijing Boxbio Technology Co., Ltd., Beijing, China). The total sulfhydryl content was calculated following eq. (2).

$$\text{Total sulfhydryl content } (\mu\text{mol/g}) = \frac{x \times V}{W} \tag{2}$$

In this equation, $x$ is the sulfhydryl content obtained from the standard curve (μmol/mL); $V$ is the volume of the sample added (1.0 mL); and $W$ is the weight of the snakehead used for the extraction of myofibrillar protein (g).

The bromophenol blue (BPB) binding method was used to analyze the surface hydrophobicity of MP (Zeng et al., 2024). BPB solution (200 μL, 1.0 mg/mL) was mixed with 1.0 mL of MP solution (5.0 mg/mL). The mixture was shaken adequately for 10 min at room temperature and then centrifuged at 5000 r/min for 15 min. The supernatant was diluted 10 times with 20 mM Tris buffer (pH 7.0) to measure the absorbance at a wavelength of 595 nm. The content of BPB bound in the supernatant was expressed as the surface hydrophobicity of MP, and it was calculated following an eq. (3).

$$\text{BPB bound}(\mu g) = 200\ \mu g \times \frac{A_0 - A_1}{A_0} \tag{3}$$

In this equation, $A_0$ is the absorbance value of 20 mM Tris buffer, Abs; $A_1$ is the absorbance value of the sample solution.

#### 2.6.3. Determination of $Ca^{2+}$-ATPase activity and intrinsic fluorescence spectra

The changes in $Ca^{2+}$-ATPase activity of MP from surimi during freeze-thaw cycle were determined by a $Ca^{2+}$-ATPase assay kit (Nanjing Jiancheng Biochemical Institute, Nanjing, China). The inorganic phosphorus content (U/mg prot) could reflect the magnitude of enzyme activity, and the procedure was followed stepwise according to the kit instructions.

MP was diluted to an appropriate concentration (0.10 mg/mL) with 0.5.0 M KCl-20 mM Tris buffer (pH 7.0). The endogenous fluorescence spectra of the samples were measured according to previous research (Yang, Bian, Dong, Xie, & Mei, 2024) using an RF-5301PC fluorescence spectrophotometer (Shimadzu CO. LTD., Kyoto, Japan) to investigate the variation in the ambient conditions of the characteristic amino acids in proteins. Spectral data of 300 to 400 nm were obtained at 295 nm excitation wavelength.

#### 2.6.4. Observation of the microstructure of fillets

The microstructure of muscle was observed following the method of the previous study (Cao et al., 2023). Frozen samples (2.0 × 2.0 × 0.5 $cm^3$) were fixed in 4.0 % paraformaldehyde solution (*v/v*) for 24 h. Gradient dehydration by 70–100 % alcohol was followed by immersion in a 1:1 mixture of anhydrous ethanol and xylene for 10 min, and xylene for 20 min. After paraffin embedding, sectioning, and hematoxylin-eosin dye staining treatment, images were acquired with an ECLIPSE E100 microscope (Nikon, Japan) at 10× magnification.

### 2.7. Separation and purification of pk1

To investigate the action mechanism of antifreeze peptide, the pk1 fraction was further separated and purified by gel chromatography. The pk1 samples were separated on a Sephadex G-15 column (1.6 cm × 80 cm), and ultrapure water was used as the eluent at a flow rate of 3.0 mL/min, with a detection wavelength of 220 nm. The separated fractions were collected and lyophilized. The THA of each fraction was determined and the method of THA analysis was described in section 2.5.

### 2.8. Peptide sequence analysis of purified products

The fraction with the highest THA after Sephadex G-15 gel chromatography separation was further characterized by mass spectrometry to identify its peptide sequence. The liquid chromatography and mass spectrometry conditions were set according to the method of Liu et al. (2024). Mobile phase A and mobile phase B were 0.1 % formic acid aqueous solution and 80 % acetonitrile/0.1 % formic acid aqueous solution, respectively. The analysis time per sample was 66 min at a flow rate of 600 nL/min. The resolution of the primary and secondary mass spectra was 70,000 and 17,500, respectively, with the scanning range set from 300 to 1800 *m/z*. The raw files of mass spectra were profiled with the software PEAKS Studio 10.6. The physicochemical properties of the peptides were organized according to the peptide sequences using the Bioladder and ProtParam websites. The grand average of peptide hydropathicity was calculated with the Expasy-ProtParam tool.

### 2.9. Prediction and modeling of antifreeze activity

All identified peptides were uploaded to the Cryoprotect antifreeze activity prediction platform (http://codes.bio/cryoprotect/) for screening peptide sequences with potential antifreeze activity among shrimp antifreeze peptides. Additionally, the structural model of the antifreeze peptide was constructed based on the AlphaFold2 website (AlphaFold Protein Structure Database).

### 2.10. Molecular docking of antifreeze peptides with water molecules

The binding capacity and interactions between antifreeze peptides and water molecules were explored through molecular docking. The structure of the water molecule was obtained from the Pubchem database with Pubchem ID 962. The peptide chains were modeled using Alphafold software, and then the peptides were docked with water molecules in Autodock vina 1.1.2 software. Meanwhile, the forces between the water molecules and low-molecular weight peptides were calculated. The conformations of low-molecular weight peptides bound to water molecules were plotted using PyMOL software.

### 2.11. Statistical analysis

Each test was repeated at least three times and all data were reported as mean ± SD. Duncan ANOVA analysis was performed using SPSS 26.0 with a significance level of $p < 0.05$. Graphs were generated by Origin 2023.

## 3. Results and discussion

### 3.1. Ultrafiltration fractionation of autolysates of shrimp head

Ultrafiltration is a method that utilizes ultrafiltration membranes to classify products based on molecular weights (Ansari et al., 2024). The DSC heat flow curves of each component after ultrafiltration fractionation are shown in Fig. 1A. At the retention temperature of 1.2 °C, exothermic peaks appeared successively in different groups. The first peak appeared in the control (BSA), while the exothermic peaks of molecular weight < 3, 3–5, 5–8, and > 8 kDa fractions were delayed. The THA value is positively correlated with the time it takes for the solution to crystallize completely (Cao et al., 2023). The THA values of <3, 3–5, 5–8, and > 8 kDa fractions were 1.95, 1.59, 1.30, and 1.16 °C, respectively (Fig. 1B). Obviously, the antifreeze activity of shrimp head autolysate was positively correlated with the molecular weight of the fractions. In this case, the higher THA value in the reaction system showed a lower ice crystal content ($\Phi$ value). The highest THA value (0.60 °C) was observed in the <3 kDa fractions prepared from silver carp hydrolysates compared to other fractions. This suggested that the antifreeze mechanism was related to the adsorption inhibition process (Luo et al., 2023). Therefore, antifreeze peptides with low-molecular weights not only bind easily with ice crystals to inhibit their growth, but also form hydrogen bonds with water molecules to hinder the ice crystal formation (Zhang, Hu, Sun, Li, & Chen, 2020). Meanwhile, the results of Table S1 also demonstrated that the <3 kDa fraction was rich in amino acid residues associated with antifreeze activity, such as aspartic acid (Asp), glutamic acid (Glu), alanine (Ala), and glycine (Gly) (Chen et al., 2022). These hydrophilic amino acid residues could combine with water molecules through hydrogen bonding, facilitating the conversion of free water to a bound water state and binding with ice crystals to exert antifreeze action.

### 3.2. Separation and characterization of less than 3 kDa molecular weight fractions

Two fractions, referred to as pk1 and pk2, were obtained from specific fractions (<3 kDa) by separating on a Capto Q anion-exchange chromatography column (Fig. 1C). The THA results indicated that the antifreeze activity of pk1 (2.28 °C) was significantly higher than that of pk2 (Fig. 1 D). There was no difference in the pk2 fraction compared to the pre-isolation period, suggesting that the increased activity of pk1 might be attributed to the enrichment of highly active peptides during the purification process. The amino acid sequence of pk1 which exhibited higher antifreeze activity, was further analyzed. The results, as shown in Table 1, demonstrated a significant increase in the glycine and alanine content of the pk1 fraction, and the residues of these two amino acids significantly increased the ice-binding capacity and freezing resistance (Yang et al., 2022). Thus, the pk1 fraction was selected for further activity validation experiments.

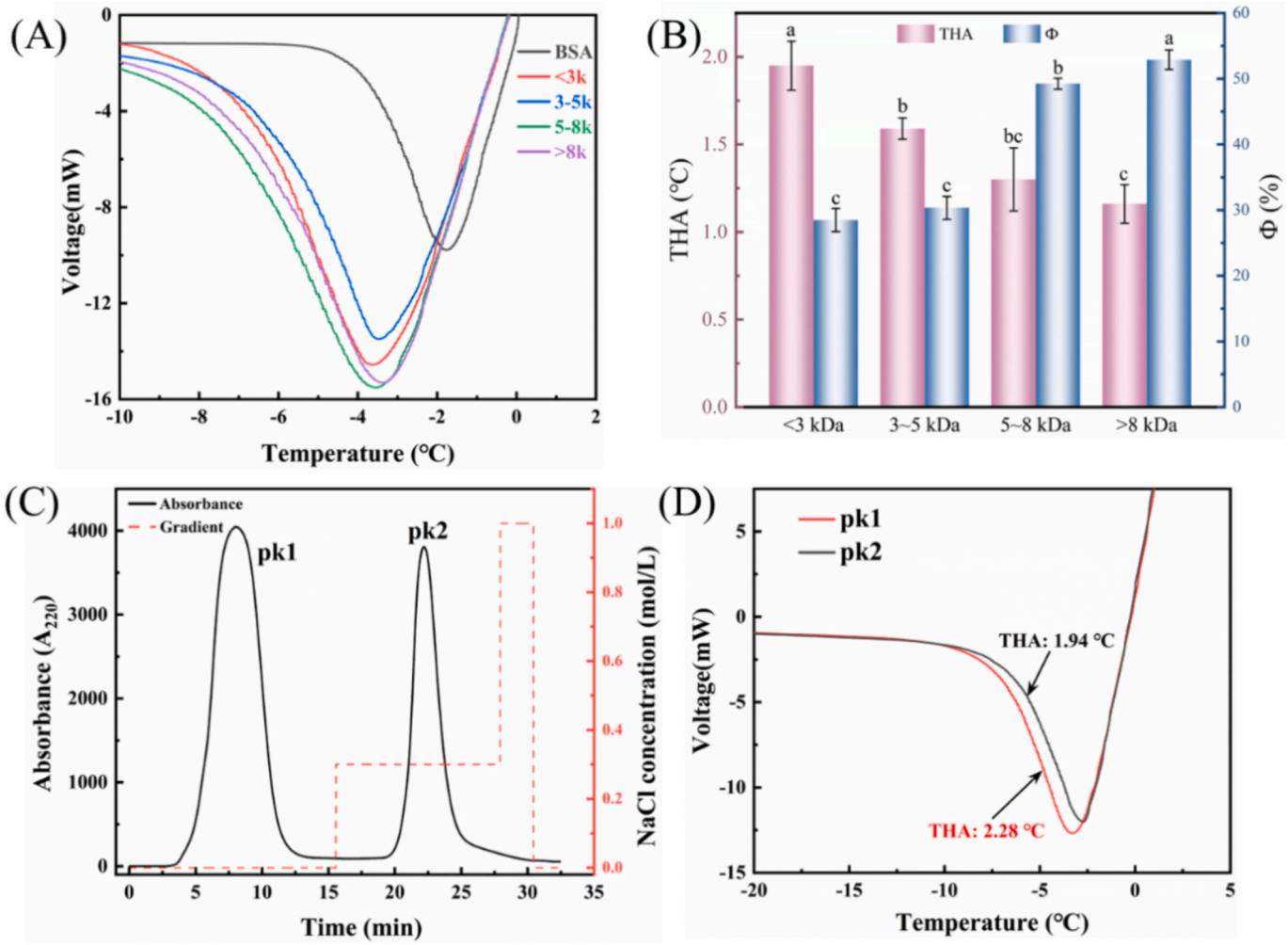


**Fig. 1.** (A) DSC heat flow curves of ultrafiltration fractionation from autolysate. (B) THA and Φ of ultrafiltration fractionation from autolysate. (C) Capto Q elution curve of ultrafiltration fractions with less than 3 kDa molecular weight (MW) obtained from autolysate. (D) DSC heat flow curves of pk1 and pk2. Different lowercase letters indicate significant differences ($p < 0.05$).

**Table 1**
The amino acid composition of pk1 and pk2 separated from MW <3 kDa.

| Animo acid | Amino acid content of separated peptides (mg/g) | |
|---|---|---|
| | pk1 | pk2 |
| Asp | 15.33 | 75.01 |
| Glu | 25.40 | 136.87 |
| Ser | 6.62 | 24.99 |
| His | 13.74 | 9.81 |
| Gly | 49.30 | 38.51 |
| Thr | 19.45 | 26.26 |
| Arg | 37.91 | 6.78 |
| Ala | 45.64 | 24.06 |
| Tyr | 28.52 | 10.61 |
| Cys | 14.90 | 12.07 |
| Val | 36.56 | 27.22 |
| Met | 19.35 | 6.38 |
| Trp | 3.54 | 1.91 |
| Phe | 40.56 | 13.10 |
| Ile | 33.34 | 9.92 |
| Leu | 67.04 | 22.39 |
| Lys | 39.09 | 24.12 |
| Pro | 32.27 | 40.68 |
| Total | 528.54 | 510.68 |

### 3.3. Cryo-protective effect of pk1 fraction on snakehead muscle during freeze-thaw cycles

#### 3.3.1. Total sulfhydryl content

Sulfhydryl groups situated at the head of myosin are readily exposed to the protein surface during freeze-thaw (F-T) cycles and can be oxidized to form disulfide bonds, resulting in a decrease in the total sulfhydryl content (Yang et al., 2023). Fig. 2A presents the changes in total sulfhydryl content of snakehead surimi impregnated with different additives during F-T cycles. The initial total sulfhydryl content of fresh samples was 3.18 μmol/g, and all samples exhibited a significant decrease in total sulfhydryl content with the increase in the number of F-T cycles. Notably, the total sulfhydryl content of pk1 and complex phosphate (PC) decreased significantly slower than that of the distilled water (NC) ($p < 0.05$). Furthermore, the antifreeze effect of pk1 was concentration-dependent. After five F-T cycles, 3.0 % pk1 displayed the optimal total sulfhydryl content. The amino acid residues in pk1 contained a large number of hydroxyl groups, which improved protein stability by adsorbing free water (Gao, Huang, Zeng, & Brennan, 2019). Cao et al. (2023) revealed that 0.5–3.0 g/100 g of tilapia skin collagen hydrolysate effectively reduced the change in total sulfhydryl content of scallop adductors, with a clear dependence of cryo-protective effect on the amount of additive.

#### 3.3.2. Surface hydrophobicity

Surface hydrophobicity serves as an indicator of conformational changes in protein structure, which is a sensitive measure of the degree of MP denaturation (Tan, Ding, Mei, & Xie, 2022). As shown in Fig. 2B, the surface hydrophobicity of MP in the NC group increased dramatically with the number of F-T cycles ($p < 0.05$), suggesting that F-T cycles led to the unfolding of the protein conformation and promoted the exposure of hydrophobic amino acids inside the protein. As a whole, the amount of BPB bound in all treatment groups was considerably lower than that in the NC after the same number of F-T cycles. This suggests that the antifreeze treatments inhibited the ice recrystallization and solute concentration effects induced by the F-T cycles to a certain extent, which effectively decreased freeze denaturation of MP and improved the quality of surimi. The addition of 0.5 % polyphosphate was comparable to 3.0 % pk1, both providing excellent control of the increase in MP surface hydrophobicity. The high proportion of hydrophilic amino acids enhanced the interaction with water molecules, retarded ice crystal growth, and reduced the conformational changes of MP (Cao et al., 2023). Further, amino acid residues in pk1 may bind to water molecules around the protein, further stabilizing MP.

#### 3.3.3. $Ca^{2+}$-ATPase activity

$Ca^{2+}$-ATPase activity is closely related to the structural integrity of the myosin globular head. The lower the $Ca^{2+}$-ATPase activity, the more severe the protein denaturation induced by the F-T cycle (Zheng, Shi, Yang, & Guo, 2023). After multiple F-T cycles, the lowest $Ca^{2+}$-ATPase activity and the largest decrease rate was observed in MP without cryoprotectant (Fig. 2C). Generally, myosin, especially the globular head responsible for $Ca^{2+}$-ATPase activity, undergoes aggregated and denatured during F-T cycle (Kittiphattanabawon, Benjakul, Visessanguan, & Shahidi, 2012). After five F-T cycles, the $Ca^{2+}$-ATPase activity was 0.1676, 0.1894, 0.1808, 0.1877, and 0.1911 U/mg prot for the NC, PC, 0.5 % pk1, 1.0 % pk1, and 3.0 % pk1, respectively. The enzyme activity of the NC group decreased fastest to 69 % of the fresh sample. It could be inferred that treatment with pk1 inhibited ice crystal recrystallization and maintained $Ca^{2+}$-ATPase activity. Ouyang et al. (2024) prepared tilapia skin collagen peptides (Gln-AFP) *via* enzymatic supramolecular assembly, which displayed a stronger cryo-protective effect on surimi than commercial antifreeze. Additionally, the inhibition effect on $Ca^{2+}$-ATPase activity loss was enhanced by a higher concentration of Gln-AFP. $Ca^{2+}$-ATPase activity has been reported to be strongly associated with sulfhydryl groups in the myosin globule head (Li, Wang, Gao, Mei, & Xie, 2021). Thus, the decreasing trend in $Ca^{2+}$-ATPase activity was similar to that of sulfhydryl content.

#### 3.3.4. Fluorescence spectra

When the protein tertiary structure unfolds, the intrinsic tryptophan residues change from original hydrophobic region to a hydrophilic environment, resulting in fluorescence quenching (Yu, Liu, Liu, Wen, & Sun, 2024). As shown in Fig. 2D, the maximum fluorescence intensity ($FI_{max}$) of MP decreased significantly after one F-T cycle compared to fresh samples, with notable difference between these treatments. This reduction could be attributed to a significant reduction of protein hydration caused by freeze-thaw treatment, resulting in unfolding of peptide chains and fluorescence bursting of tryptophan residues (Yang et al., 2023). The cryo-protective effect of pk1 and commercial cryoprotectants were again illustrated as the number of F-T cycles increased, especially at 3.0 % pk1 (Fig. 2E). The analysis indicated that pk1 provided a protective barrier for MP conformational stability.

#### 3.3.5. Microstructure

Fig. 2F presents micrographs of antifreeze-treated snakehead fillets after different F-T cycles. Bulky and irregularly shaped ice crystals cause severe damage to muscle tissue structure (Tan, Ye, Chu, & Xie, 2021). It was observed that the surface of fresh fillets had a dense and smooth fiber network structure. In contrast, the microstructure of fillets in the NC group was seriously destroyed after F-T cycles treatment, with a gradual increase in muscle interstices. Even large cracks appeared in the late stage, and the surface became disordered and non-regular. However, the gaps between fillet muscle fibers treated with the pk1 and complex phosphates were denser than in the NC group. It was demonstrated that pk1 and complex phosphates reduced the formation of large ice crystals and minimized the mechanical damage caused by irregular ice crystal formation to muscle tissue. It may be summarized that pk1 effectively retarded the microfilm disintegration of snakehead fillets caused by the F-T cycles, comparable to complex phosphates.

### 3.4. Separation and purification of high activity fraction pk1

After pk1 was separated by the Sephadex G-15 gel filtration column, three fractions (marked as pk1-A, pk1-B, and pk1-C) were obtained as shown in Fig. 3A. The elution results demonstrated that pk1-A had the highest molecular mass, followed by pk1-B and pk1-C. Notably, the thermal hysteresis activity (THA) of all three grades was significantly increased compared to the pk1 before fractionation (2.28 °C) (Fig. 3B). This increase in THA could be attributed to the increased purity of the antifreeze actives components after fractionation. Among these

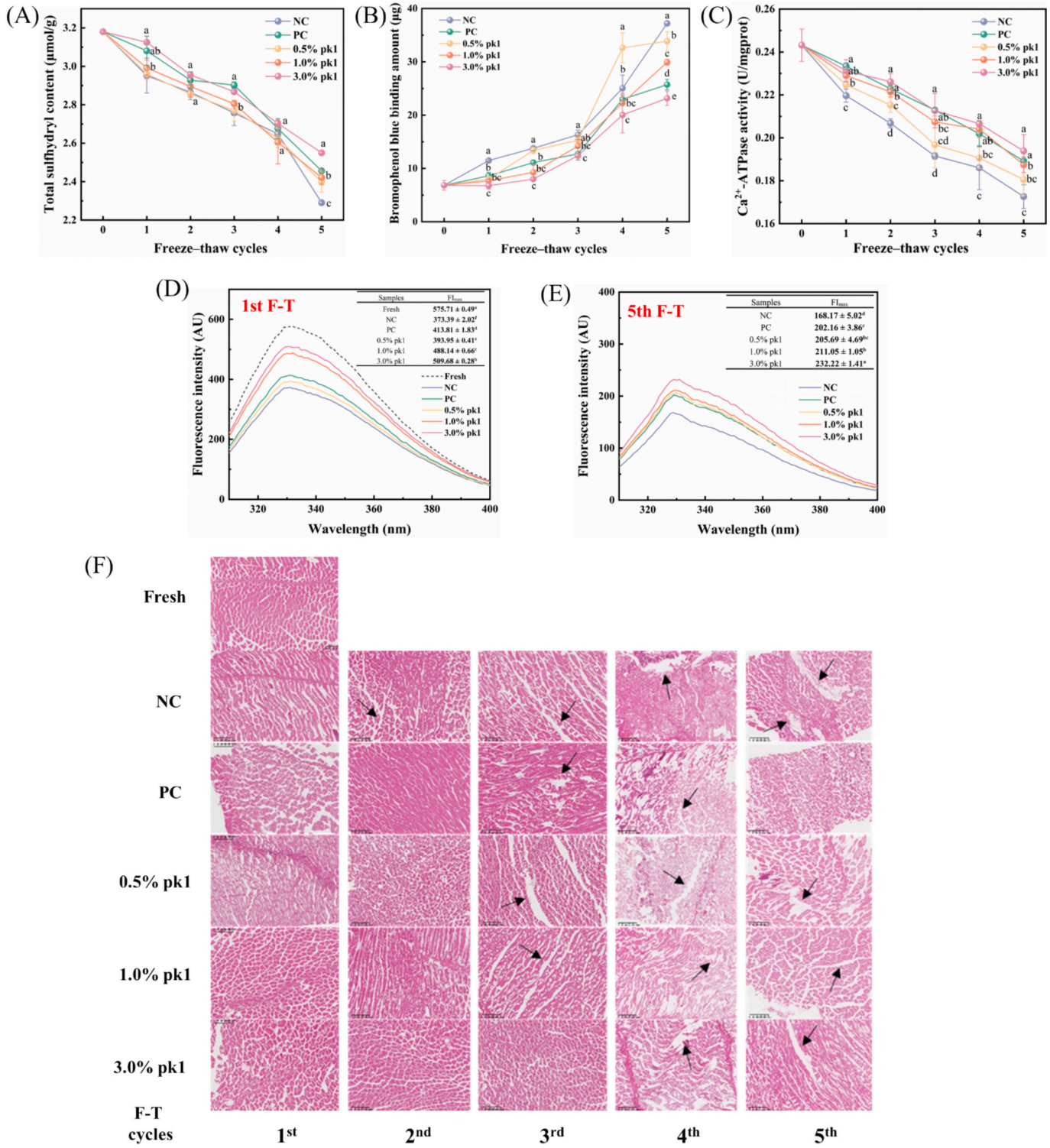


**Fig. 2.** Total sulfhydryl content (A), surface hydrophobicity (B), $Ca^{2+}$-ATPase activity (C), fluorescence intensity of 1st F-T (D), fluorescence intensity of 5th F-T (E) and microstructure (F, magnification of 10×) of snakehead muscle with different treatments as affected by freeze-thaw cycles. Different lowercase letters within the same freeze-thaw cycle indicate significant differences ($p < 0.05$).

fractions, the large molecular weight fraction pk1-A showed the highest THA (2.80 °C). Peptides isolated from gelatin hydrolysates had the highest THA (5.19 °C) when the molecular weight was 1.7–4.2 kDa, whereas those with molecular weights of 4.9–10.3 kDa (4.27 °C) and 0.4–1.4 kDa (4.22 °C) showed similar THA values (Kittiphattanabawon, Sriket, Nalinanon, Visessanguan, & Benjakul, 2024). The results indicated that the AFP with highly active pk1 mainly existed in pk1-A, and pk1-A played a key role in the cryoprotection of surimi in F-T cycles.

### 3.5. *Peptide sequence of the purified product pk1-a*

The peptide sequence of the pk1-A fraction with the highest antifreeze activity was analyzed by LC-MS/MS (Fig. 3C). A total of 1144 peptides were subsequently identified *via* the protein database. Table S2

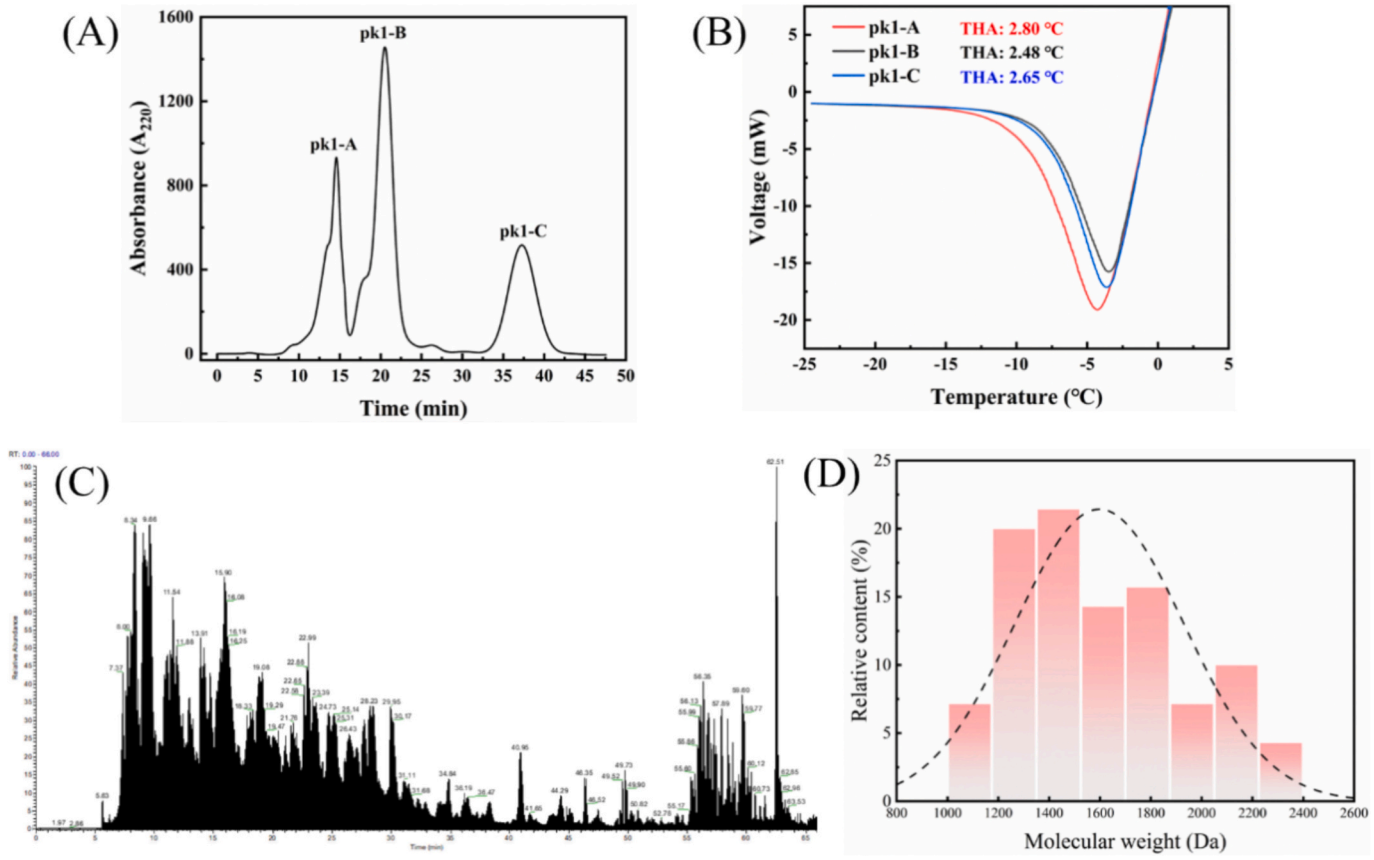


**Fig. 3.** (A) Sephadex G-15 elution curve of pk1. (B) DSC heat flow curves of pk1 separation fractions. (C) Total ion flow chromatogram of pk1-A by LC-MS/MS. (D) The molecular weight distribution of 70 peptides with high confidence.

**Table 2**
Prediction of selected peptides by Cryoprotect platform.

| No. | Peptide sequence | Length | Protein Accession | Position | Prediction |
|---|---|---|---|---|---|
| 1 | IKDHAATSMTNGK | 13 | tr\|A0A423SNE1\|A0A423SNE1_PENVA | 871–883 | AFP |
| 2 | YGSHGVYPDK | 10 | tr\|X2KWE4\|X2KWE4_PENVA | 615–624 | AFP |
| 3 | GSVKVHAQGH | 10 | tr\|A0A3R7M1N6\|A0A3R7M1N6_PENVA | 229–238 | AFP |
| 4 | YGSHGKYPDNRPHG | 14 | tr\|A0A3R7Q123\|A0A3R7Q123_PENVA | 628–641 | AFP |
| 5 | KQVHPDTGISSK | 12 | tr\|A0A3R7PKU8\|A0A3R7PKU8_PENVA | 261–272 | AFP |
| 6 | HGKYPDNRPHG | 11 | tr\|A0A3R7Q123\|A0A3R7Q123_PENVA | 631–641 | AFP |
| 7 | AHGKYPDNRPH | 11 | tr\|A0A423SGU8\|A0A423SGU8_PENVA | 1290–1300 | AFP |
| 8 | YGSHGKYPDNRP | 12 | tr\|A0A3R7Q123\|A0A3R7Q123_PENVA | 628–639 | AFP |
| 9 | YGSHGKYPDNRPH | 13 | tr\|A0A3R7Q123\|A0A3R7Q123_PENVA | 628–640 | AFP |
| 10 | GSHGKYPDNRP | 11 | tr\|A0A3R7Q123\|A0A3R7Q123_PENVA | 629–639 | AFP |
| 11 | GSHGVYPDKR | 10 | tr\|X2KWE4\|X2KWE4_PENVA | 616–625 | AFP |
| 12 | NHYGSHGVYPDK | 12 | tr\|X2KWE4\|X2KWE4_PENVA | 613–624 | AFP |
| 13 | HYGSHGVYPDK | 11 | tr\|X2KWE4\|X2KWE4_PENVA | 614–624 | AFP |
| 14 | TGTKKNPEQRVA | 12 | tr\|X2KWE4\|X2KWE4_PENVA | 185–196 | Non-AFP |
| 15 | YGSHGVYPDKRPH | 13 | tr\|X2KWE4\|X2KWE4_PENVA | 615–627 | AFP |
| 16 | YGSHGVYPDKRP | 12 | tr\|X2KWE4\|X2KWE4_PENVA | 615–626 | AFP |
| 17 | HYGSHGKYPDN | 11 | tr\|A0A3R7Q123\|A0A3R7Q123_PENVA | 627–637 | AFP |
| 18 | HYGSHGKYPD | 10 | tr\|A0A3R7Q123\|A0A3R7Q123_PENVA | 627–636 | AFP |
| 19 | GSHGKYPDKRPH | 12 | tr\|A0A3R7N5I8\|A0A3R7N5I8_PENVA | 550–561 | AFP |
| 20 | GSHGVYPDKRPH | 12 | tr\|X2KWE4\|X2KWE4_PENVA | 616–627 | AFP |
| 21 | GSHGVYPDKRP | 11 | tr\|X2KWE4\|X2KWE4_PENVA | 616–626 | AFP |
| 22 | SHGVYPDKRPH | 11 | tr\|X2KWE4\|X2KWE4_PENVA | 617–627 | AFP |
| 23 | KSSFTGTKKNPEQ | 13 | tr\|X2KWE4\|X2KWE4_PENVA | 181–193 | AFP |
| 24 | SSFTGTKKNPEQR | 13 | tr\|X2KWE4\|X2KWE4_PENVA | 182–194 | AFP |
| 25 | HYGSHGKYPDNRPH | 14 | tr\|A0A3R7Q123\|A0A3R7Q123_PENVA | 627–640 | AFP |
| 26 | NHYGSHGKYPDNRP | 14 | tr\|A0A3R7Q123\|A0A3R7Q123_PENVA | 626–639 | AFP |
| 27 | SSFTGTKKNPEQ | 12 | tr\|X2KWE4\|X2KWE4_PENVA | 182–193 | AFP |
| 28 | HGVYPDKRPH | 10 | tr\|X2KWE4\|X2KWE4_PENVA | 618–627 | Non-AFP |
| 29 | VFNHGEHIHH | 10 | tr\|A0A3R7NPL9\|A0A3R7NPL9_PENVA | 668–677 | Non-AFP |

summarizes 70 peptides with high confidence in LC-MS/MS. Notably, the amino acid sequence YPD appeared multiple times among these sequences. This sequence differs from the Gly-rich tripeptide repeat sequence (Gly-XY) in collagen-based antifreeze peptides, likely due to the differing protein sources (Zhang, Wang, Yang, & Chen, 2024). The proline (P) and aspartic acid (D) in the pk1-A fraction interacted with water molecules to form a glassy state. Y. Zhang et al. (2024) revealed through molecular simulations that proline inhibited the ice crystal formation by forming hydrogen bonds with water, which effectively reduced the harmful effects of ice crystals on shrimp muscles. In general, the molecular weight of peptides is correlated with their antifreeze activity (Liu et al., 2024). As shown in Fig. 3D, the molecular weight distribution of the 70 identified peptides was primarily concentrated in the range of 1300–1800 Da, which was similar to the published data on the molecular weights of shrimp head antifreeze peptides (Majura et al., 2023; Zhu et al., 2022). This distribution was compatible with the molecular weight characteristics of antifreeze peptides, and smaller molecular weights were more indicative of higher antifreeze activity. Nevertheless, not all of these peptides necessarily belong to AFP, so further screening and activity prediction are required.

### 3.6. Prediction and modeling of potential antifreeze activity

When a peptide exhibits an instability index >40, it indicates poor stability *in vitro* and hence be excluded as a potential antifreeze candidate (Zhu et al., 2022). Furthermore, peptides with lengths between 7 and 14 amino acids are considered an optimal for antifreeze peptides. Based on these principles, a total of 29 peptide sequences were screened for further analysis. These sequences were then uploaded to Cryoprotect, an antifreeze peptide activity prediction platform, to predict which belonged to the AFP (Cui et al., 2023). From Table 2, it could be noticed that 26 peptides were identified as potential AFPs. Notably, these 26 peptides exhibited a high content of glycine (15 %) and proline (12 %). The sequences were derived from 6 protein accessions. Consequently, one peptide was randomly selected from each protein accession, with the following sequences: IKDHAATSMTNGK, YGSHGVYPDK, GSVKVHAQGH, YGSHGKYPDNRPHG, KQVHPDTGISSK, and AHGKYPDNRPH. The molecular structures of these 6 peptide sequences were modeled using AlphaFold 2, as illustrated in Fig. 4A.

### 3.7. Molecular docking to simulate the interaction between antifreeze peptides and water molecules

In recent years, studies based on molecular simulation techniques have been effectively applied to characterize the structural conformation of antifreeze proteins and their interaction mechanism with water molecules (Jiang et al., 2022). To investigate the antifreeze mechanism of shrimp head antifreeze peptide, this study predicted the three-dimensional structure of 6 peptide chains using this tool (Fig. 4A) Fig. 4A depicts potential peptide-water binding modes. By analysis, it was found that the interaction between the antifreeze peptide and the surrounding water molecules occurs *via* hydrogen bonding, yet the variation in the number of hydrogen bonds depends on peptide sequences. Typically, when the binding energy is <0, it can be assumed that the binding process between peptides and water molecules is spontaneous (Liu et al., 2024). The lower binding energy suggests the higher degree of spontaneous binding, and the final formation of the ice-binding system is more stable. The binding energies between the water molecules and peptides after docking were all <0 (Table 3), indicating that these 6 peptides were able to spontaneously bind to water molecules. More importantly, KQVHPDTGISSK exhibited the best binding capacity (−1.8 kcal/mol). Hence, KQVHPDTGISSK was selected as the polypeptide sequence with the highest antifreeze potential among the shrimp head antifreeze peptides and named as *Litopenaeus vannamei* head antifreeze peptide (LvAFP).

To deeply reveal the action sites and potential mechanisms between LvAFP and water molecules, the specific conformation between the two molecules was plotted using PyMOL software, as shown in Fig. 4B. The results demonstrated that the presence of hydrogen bonding between the two molecules, except in conformation P8. Subsequently, we searched for the optimal binding conformation of LvAFP when docked with water molecules.

Among these conformations, P1 exhibited the highest number of hydrogen bonds (5) with water molecules, followed by P2 (4), P5 (3), P3 (2), P6 (2), and P7 (2). Those with only 1 hydrogen bond were P4 and P9. Evidently, the P1 conformation demonstrated the greatest stability in binding to water molecules, correlating with its high antifreeze activity. For conformation P1, water molecules could bind to the Lys residue at position 12 of LvAFP *via* 2.2 and 2.3 Å hydrogen bonds, respectively, to the Thr residue at position 7 *via* 2.4 and 2.7 Å hydrogen bonds, respectively, and to the Asp residue at position 6 *via* 2.4 Å hydrogen bonds. In the conformation P2, the water molecule bound to the Lys residue at position 12 through 2.1, 2.4, and 2.5 Å hydrogen bonding, respectively, and to the Thr residue at position 7 with 2.6 Å hydrogen bonding. Similar binding to lysine residues at position 1 or 12 was observed in P3, P4, P5, P7, and P9. The results indicated that the presence of Lys residues in LvAFP may serve as a pivotal factor contributing to its antifreeze activity, especially at the binding site of Lys 12. Additionally, it could be noticed from Table 1 that the Lys content in pk1, which had a higher THA, was significantly higher than that in pk2. Relevant evidence also demonstrated that antifreeze peptides may inhibit ice recrystallization by repelling water molecules *via* hydrophobic interactions formed by hydrophobic amino acids (Yang et al., 2022). It could be deduced that the antifreeze mechanism of LvAFP was closely related to its amino acid composition. There are strong binding interactions between water molecules and LvAFP due to the presence of hydrogen bonding, serving to inhibit the growth and recrystallization of ice crystals.

## 4. Conclusion

In this study, peptides were extracted from shrimp (*Litopenaeus vannamei*) heads by ultrasound-assisted autolysis. Peptides with antifreeze activity were then identified and characterized using traditional method, bioinformatics, and molecular simulation. The results revealed that the fraction with a molecular weight of <3 kDa exhibited significant antifreeze activity, with significantly higher THA (1.95 °C) than others fractions. This attributed to the presence of a large number of hydrophilic amino acid residues. The pk1 fraction (THA of 2.28 °C) which was separated from the <3 kD fraction was found to be effective in retarding the protein denaturation of snakehead muscle during freeze-thaw cycles. The addition of 0.5 % polyphosphate demonstrated a comparable effect to that of 3.0 % PK1, with both effectively inhibiting MP freeze denaturation. After pk1 was separated and purified by Sephadex G-15, the component pk1-A exhibited the highest activity, with a THA reaching 2.80 °C. The results of peptide identification indicated that the sequence YPD appeared multiple times in 70 peptides with high confidence. 26 peptides were identified as AFP through bioinformatic tool, with glycine and proline accounting for 15 % and 12 % of the sequences, respectively. Molecular docking analysis identified the peptide KQVHPDTGISSK as a potential antifreeze peptide. Furthermore, the active site (Lys12) on KQVHPDTGISSK displayed a strong binding affinity for water molecules, interacting mainly *via* hydrogen bonding, which contributed to the inhibition of ice crystal formation. Consequently, antifreeze peptide derived from the shrimp head (LvAFP) could serve as a potential alternative cryo-protectant in frozen snakehead or aquatic food, reducing the extensive use of mixed phosphates in frozen foods preservation.

## CRediT authorship contribution statement

**Mingtang Tan:** Writing – original draft, Visualization, Methodology, Investigation, Funding acquisition, Formal analysis, Conceptualization.

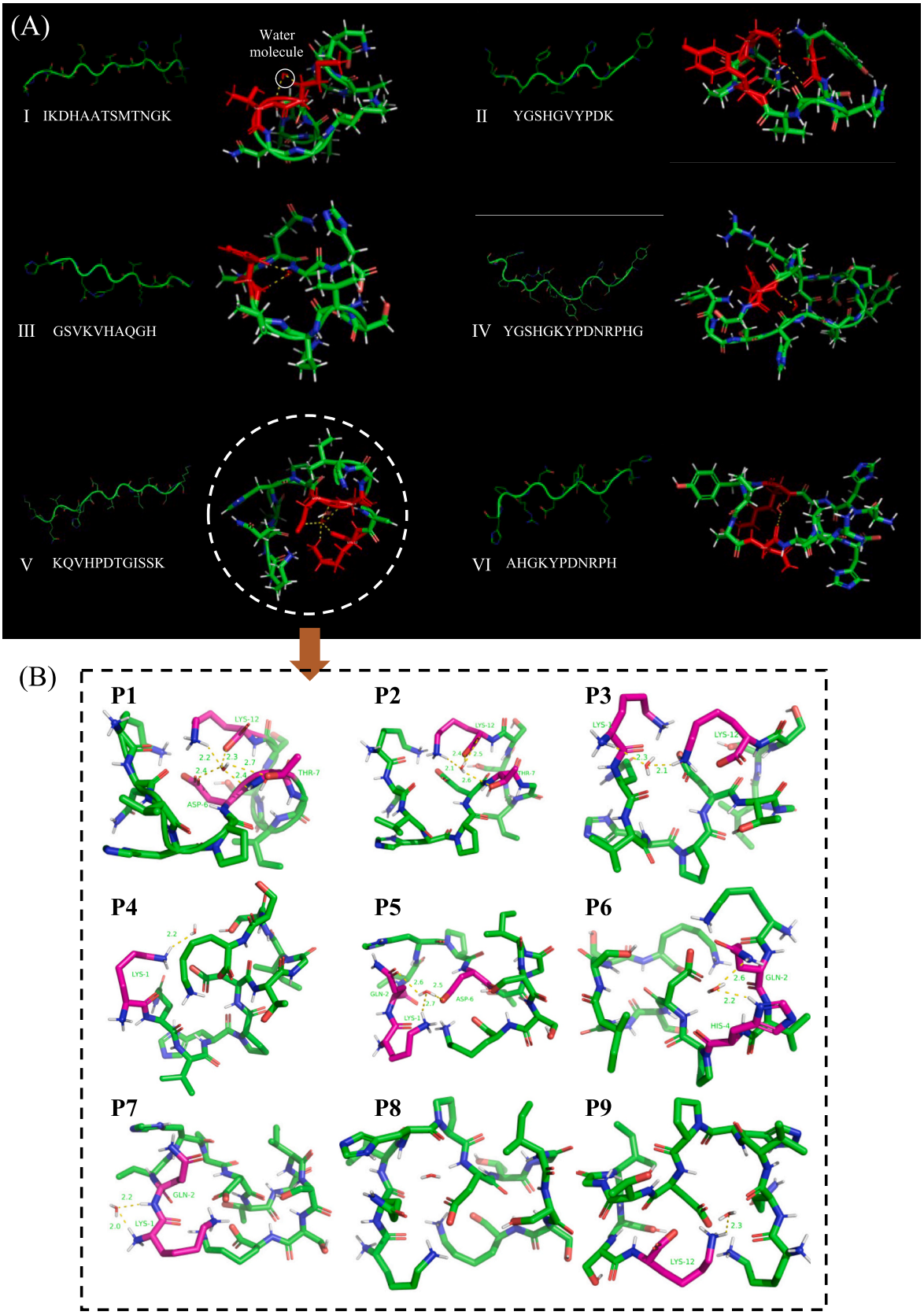


**Fig. 4.** (A) Predictive molecular structures of 6 antifreeze peptide sequences and interactions with water molecules. (B) Molecular docking results of LvAFP (peptide sequence KQVHPDTGISSK) with water molecules.

**Table 3**
The binding sites and binding energies of 6 peptides with water molecules.

| Peptide | Center x | Center y | Center z | Binding energy(kcal/mol) |
|---|---|---|---|---|
| IKDHAATSMTNGK | 8.902281 | 17.591609 | −13.596141 | −1.2 |
| YGSHGVYPDK | 8.215498 | 19.690147 | −8.523763 | −1.3 |
| GSVKVHAQGH | 8.763735 | 13.768947 | −8.043053 | −1.1 |
| YGSHGKYPDNRPHG | 8.215498 | 19.690147 | −8.523763 | −0.9 |
| KQVHPDTGISSK | 14.105303 | 8.466308 | −12.8684 | −1.8 |
| AHGKYPDNRPH | 5.851903 | 16.162503 | −7.620669 | −1.2 |

**Mei Han:** Software, Methodology, Investigation, Data curation. **Yingyu Zhou:** Software, Methodology, Investigation. **Zhongqin Chen:** Software, Methodology. **Wenhong Cao:** Writing – review & editing, Validation, Supervision, Project administration, Funding acquisition.

## Declaration of competing interest

The authors declare that they have no known competing financial interests or personal relationships that could have appeared to influence the work reported in this paper.

## Acknowledgments

This work was supported by the National Natural Science Foundation of China (Grant No. 32172163) and the Program for scientific research start-up funds of Guangdong Ocean University (060302042314).

## Appendix A. Supplementary data

Supplementary data to this article can be found online at https://doi.org/10.1016/j.fochx.2025.102395.

## Data availability

Data will be made available on request.

## References

Ansari, F., Tafti, H., Amanzadeh, A., Rabbani, S., Shokrgozar, M., Heidari, R., Behroozi, J., Eyni, H., Uversky, V., & Ghanbari, H. (2024). Comparison of the efficiency of ultrafiltration, precipitation, and ultracentrifugation methods for exosome isolation. *Biochemistry and Biophysics Reports, 38*, Article 101668. https://doi.org/10.1016/j.bbrep.2024.101668

Cao, L., Majura, J. J., Liu, L., Cao, W., Chen, Z., Zhu, G., … Lin, H. (2023). The cryoprotective activity of tilapia skin collagen hydrolysate and the structure elucidation of its antifreeze peptide. *LWT, 179*, Article 114670. https://doi.org/10.1016/j.lwt.2023.114670

Cao, W., Tan, C., Zhan, X., Li, H., & Zhang, C. (2014). Ultraviolet irradiation and gradient temperature assisted autolysis for protein recovery from shrimp head waste. *Food Chemistry, 164*, 136–141. https://doi.org/10.1016/j.foodchem.2014.05.042

Chen, X., Wu, J., Li, X., Yang, F., Yu, L., Li, X., Huang, J., & Wang, S. (2022). Investigation of the cryoprotective mechanism and effect on quality characteristics of surimi during freezing storage by antifreeze peptides. *Food Chemistry, 371*, Article 131054. https://doi.org/10.1016/j.foodchem.2021.131054

Chu, Y., Ding, Z., Wang, J., Xie, J., & Ding, Y. (2023). Factors affecting the quality of frozen large yellow croaker (Pseudosciaena crocea) in cold chain logistics: Retention time and temperature fluctuation. *Food Chemistry: X, 18*, Article 100742.

Cui, M., Li, J., Li, J., Wang, F., Li, X., Yu, J., Huang, Y., & Liu, Y. (2023). Screening and characterization of a novel antifreeze peptide from silver carp muscle hydrolysate. *Food Chemistry, 403*, Article 134480. https://doi.org/10.1016/j.foodchem.2022.134480

Dang, M., Wang, R., Jia, Y., Du, J., Wang, P., Xu, Y., & Li, C. (2022). The antifreeze and Cryoprotective activities of a novel antifreeze peptide from Ctenopharyngodon idella scales. *Foods, 11*(13), 1830. https://doi.org/10.3390/foods11131830

Dayakar, B., Xavier, K. A. M., Ngasotter, S., Layana, P., Balange, A. K., Priyadarshini, B., & Nayak, B. (2022). Characterization of spray-dried carotenoprotein powder from Pacific white shrimp (*Litopenaeus vannamei*) shells and head waste extracted using papain: Antioxidant, spectroscopic, and microstructural properties. *LWT, 159*, Article 113188. https://doi.org/10.1016/j.lwt.2022.113188

El Boumlasy, S., Mangraviti, D., Arena, K., Cacciola, F., Asraoui, F., & Debdoubi, A. (2024). Determination of astaxanthin and astaxanthin esters in three samples of shrimp waste (*Parapenaeus longirostris*) by high performance liquid chromatography coupled photo-diode array and mass spectrometry detection. *Natural Product Research, 38*(16), 2901–2908. https://doi.org/10.1080/14786419.2023.2245959

Gao, W., Huang, Y., Zeng, X., & Brennan, M. A. (2019). Effect of soluble soybean polysaccharides on freeze-denaturation and structure of myofibrillar protein of bighead carp surimi with liquid nitrogen freezing. *International Journal of Biological Macromolecules, 135*, 839–844. https://doi.org/10.1016/j.ijbiomac.2019.05.186

Jiang, W., Yang, F., Chen, X., Cai, X., Wu, J., Du, M., … Wang, S. (2022). Molecular simulation-based research on antifreeze peptides: Advances and perspectives. *Journal of Future Foods, 2*(3), 203–212. https://doi.org/10.1016/j.jfutfo.2022.06.002

Kittiphattanabawon, P., Benjakul, S., Visessanguan, W., & Shahidi, F. (2012). Cryoprotective effect of gelatin hydrolysate from blacktip shark skin on surimi subjected to different freeze-thaw cycles. *LWT, 47*(2), 437–442. https://doi.org/10.1016/j.lwt.2012.02.003

Kittiphattanabawon, P., Sriket, C., Nalinanon, S., Visessanguan, W., & Benjakul, S. (2024). Gelatin hydrolyzed by papaya latex enzymes as an alternative cryoprotectant for frozen raw Pacific white shrimp (*Penaeus vannamei*). *Food Bioscience, 60*, Article 104199. https://doi.org/10.1016/j.fbio.2024.104199

Li, B., Wang, X., Gao, X., Mei, J., & Xie, J. (2021). Effect of active coatings containing lippa citriodora kunth. Essential oil on bacterial diversity and myofibrillar proteins degradation in refrigerated large yellow croaker. *Polymers, 13*(11), 1787. https://doi.org/10.3390/polym13111787

Liang, J., Chen, X., Majura, J., Tan, M., Chen, Z., Gao, J., & Cao, W. (2025). Insight into the structure-activity relationship of thermal hysteresis activity of cod collagen peptides through peptidomics and bioinformatics approaches. *Food Chemistry, 463*, Article 141514. https://doi.org/10.1016/j.foodchem.2024.141514

Liu, M., Bai, S., Jiang, Z., Li, H., Tu, Z., Liao, T., Yu, W., & Qiu, L. (2024). Identification and isolation of a novel antifreeze peptide from crayfish shells. *LWT, 198*, Article 116030. https://doi.org/10.1016/j.lwt.2024.116030

Luo, W., Yuan, C., Wu, J., Liu, Y., Wang, F., Li, X., & Wang, S. (2023). Inhibition mechanism of membrane-separated silver carp hydrolysates on ice crystal growth obtained through experiments and molecular dynamics simulation. *Food Chemistry, 414*, Article 135695. https://doi.org/10.1016/j.foodchem.2023.135695

Majura, J., Chen, X., Chen, Z., Tan, M., Zhu, G., Gao, J., Lin, H., & Cao, W. (2024). The cryoprotective effect of Litopenaeus vannamei head-derived peptides and its ice-binding mechanism. *Current Research in Food Science, 9*, Article 100886. https://doi.org/10.1016/j.crfs.2024.100886

Majura, J., Han, M., Ouyang, J., Chen, X., Chen, Z., Tan, M., Gao, J., Lin, H., Zheng, H., & Cao, W. (2023). The antifreeze activity and physicochemical properties of Litopenaeus vannamei head autolysate. *International Journal of Food Science & Technology, 58*(11), 6131–6142. https://doi.org/10.1016/j.foodchem.2023.135695

Nirmal, N. P., Santivarangkna, C., Rajput, M. S., & Benjakul, S. (2020). Trends in shrimp processing waste utilization: An industrial prospective. *Trends in Food Science & Technology, 103*, 20–35. https://doi.org/10.1016/j.tifs.2020.07.001

N'Souvi, K., Sun, C., Che, B., & Vodounon, A. (2024). Shrimp industry in China: Overview of the trends in the production, imports and exports during the last two decades, challenges, and outlook. *Frontiers in Sustainable Food Systems, 7*, 1287034. https://doi.org/10.3389/fsufs.2023.1287034

Ouyang, J., Han, M., Majura, J. J., Chen, X., Tan, M., Chen, Z., … Cao, W. (2024). Improvement of the antifreeze activity of tilapia skin collagen peptides through enzymatic supramolecular assembly approach. *International Journal of Food Science & Technology, 59*(5), 3360–3372. https://doi.org/10.1111/ijfs.17082

Pacheco, A., Pacheco, F., Pereira, G., Paiva, P., Lelis, C., Tribst, A., & Leite Júnior, B. (2024). Structural changes induced by ultrasound in proteases and their consequences on the hydrolysis of pumpkin seed proteins and the multifunctional properties of hydrolysates. *Food and Bioproducts Processing, 144*, 13–21. https://doi.org/10.1016/j.fbp.2023.12.004

Sun Q, Zhang H, Yang X, et al. (2023). Insight into muscle quality of white shrimp (*Litopenaeus vannamei*) frozen with static magnetic-assisted freezing at different intensities. *Food Chemistry: X, 2023*, 17: 100518. https://Doi: https://doi.org/10.1016/j.fochx.2022.100518.

Tadesse, S., Emire, S., Barea, P., Illera, A., Melgosa, R., Beltrán, S., & Sanz, M. (2023). Valorisation of low-valued ray-finned fish (*Labeobarbus nedgia*) by enzymatic hydrolysis to obtain fish-discarded protein hydrolysates as functional foods. *Food and Bioproducts Processing, 141*, 167–184. https://doi.org/10.1016/j.fbp.2023.08.003

Tan, M., Ding, Z., Mei, J., & Xie, J. (2022). Effect of cellobiose on the myofibrillar protein denaturation induced by pH changes during freeze-thaw cycles. *Food Chemistry, 373*, Article 131511. https://doi.org/10.1016/j.foodchem.2021.131511

Tan, M., Ye, J., Chu, Y., & Xie, J. (2021). The effects of ice crystal on water properties and protein stability of large yellow croaker (*Pseudosciaena crocea*). *International Journal of Refrigeration, 130*, 242–252. https://doi.org/10.1016/j.ijrefrig.2021.05.040

Tan, M., Ye, J., & Xie, J. (2021). Freezing-induced myofibrillar protein denaturation: Role of pH change and freezing rate. *LWT, 152*, Article 112381. https://doi.org/10.1016/j.lwt.2021.112381

Wang, Y., Liu, X., Jiang, P., Qi, L., Fu, B., & Shang, S. (2024). Inhibition of protein denaturation and oxidation of prepared shrimp paste by sturgeon skin collagen peptide. *Food Bioscience, 58*, Article 103766. https://doi.org/10.1016/j.fbio.2024.103766

Xu, Z., Cao, S., Zhu, Z., Hu, B., Chen, H., Tu, M., Tan, Z., Du, M., & Li, T. (2024). Characterization and the mechanism underlying the cryoprotective activity of a peptide from large yellow croaker (*Pseudosciaena crocea*). *Food Chemistry, 435*, Article 137512. https://doi.org/10.1016/j.foodchem.2023.137512

Yang, F., Jiang, W., Chen, X., Chen, X., Wu, J., Huang, J., Cai, X., & Wang, S. (2022). Identification of novel antifreeze peptides from takifugu obscurus skin and molecular mechanism in inhibiting ice crystal growth. *Journal of Agricultural and Food Chemistry, 70*(44), 14148–14156. https://doi.org/10.1021/acs.jafc.2c04393

Yang, F., Jiang, W., Chen, X., Wu, J., Huang, J., Cai, X., & Wang, S. (2023). Investigation on the quality regulating mechanism of antifreeze peptides on frozen surimi: From macro to micro. *Food Research International, 163*, Article 112299. https://doi.org/10.1016/j.foodres.2022.112299

Yang, X., Bian, C., Dong, Y., Xie, J., & Mei, J. (2024). Effects of different power multi-frequency ultrasound-assisted thawing on the quality characteristics and protein stability of large yellow croaker (*Larimichthys crocea*). Food Chemistry: X:, 23, 101559. https://Doi: https://doi.org/10.1016/j.fochx.2024.101559.

Yu, Q., Liu, J., Liu, Y., Zheng, Y., Pi, R., Mubango, E., Tan, Y., Luo, Y., & Hong, H. (2022). Inhibitive effect of cryoprotectants on the oxidative and structural changes in myofibrillar proteins of unwashed mince from silver carp during frozen storage. *Food Research International, 161*, Article 111880. https://doi.org/10.1016/j.foodres.2022.111880

Yu, Q., Liu, S., Liu, Q., Wen, R., & Sun, C. (2024). Meat exudate metabolomics reveals the impact of freeze-thaw cycles on meat quality in pork loins. *Food Chemistry: X, 24*, Article 101804. https://doi.org/10.1016/j.fochx.2024.101804

Zeng, Q., Hu, D., Li, Y., Qi, P., Chen, L., Wang, R., Zhao, Y., & Wang, J. (2024). Conjugates of glycosylated antarctic krill proteins and curcumin: Maintaining the storage quality of salmon fillets coupling with photodynamic inactivation. *Food Hydrocolloids, 155*, Article 110191. https://doi.org/10.1016/j.foodhyd.2024.110191

Zhang, C., Wang, Y., Yang, Q., & Chen, H. (2024). Effect of bovine hide gelatin antifreeze peptides on the quality of frozen dough treated with freeze-thaw cycles and its steamed bread. *Journal of Cereal Science, 117*, Article 103924. https://doi.org/10.1016/j.jcs.2024.103924

Zhang, X., Xu, J., Tian, X., Wang, Y., Liao, X., & Zhao, L. (2024). Mechanisms of persimmon pectin methyl esterase activation by high pressure processing based on chemical experiments and molecular dynamics simulations. *Food Chemistry, 432*, Article 137239. https://doi.org/10.1016/j.foodchem.2023.137239

Zhang, Y., Chen, Z., Wang, Y., Dong, H., Sun, J., Li, J., & Mao, X. (2024). Molecular modelling studies reveal cryoprotective mechanism of L-proline during the frozen storage of shrimp (*Litopenaeus vannamei*). *Food Chemistry, 441*, Article 138259. https://doi.org/10.1016/j.foodchem.2023.138259

Zhang, Y., Hu, W., Sun, J., Li, Y., & Chen, C. (2020). Hydrogen bonds and hydrate interaction between RiAFP and water revealed by molecular dynamics simulations. *Chemical Physics, 538*, Article 110860. https://doi.org/10.1016/j.chemphys.2020.110860

Zheng, Y., Shi, Y., Yang, X., & Guo, Q. (2023). Flammulina velutipes polysaccharide improves the water-holding capacity in the dorsal muscle of freeze-thawed cultured large yellow croaker (*Larimichthys crocea*). *Food Chemistry, 403*, Article 134401. https://doi.org/10.1016/j.foodchem.2022.134401

Zhou, L., Kang, D., Wang, J., Cai, J., Xing, L., & Zhang, W. (2024). Effects of ultrasound-assisted emulsification and carboxymethyl cellulose addition on the rheological and microstructure properties of myofibrillar protein-soybean oil emulsion gel. *Food and Bioproducts Processing, 144*, 203–213. https://doi.org/10.1016/j.fbp.2024.02.003

Zhu, K., Zheng, Z., & Dai, Z. (2022). Identification of antifreeze peptides in shrimp byproducts autolysate using peptidomics and bioinformatics. *Food Chemistry, 383*, Article 132568. https://doi.org/10.1016/j.foodchem.2022.132568